Energy-Weighted Acquisition: Evaluation of Physical Characteristics and Clinical Utility

Todd Donaghy, Erin McKay, Richard Smart, Richard Quinn and S. Patrick Butler

Department of Nuclear Medicine, St. George Hospital, Kogarah, Sydney, Australia

Objective: Energy-weighted acquisition (EWA) is a commercially available technique designed to reduce the contribution of Compton scattered radiation in the final image. This study investigates the utility of EWA, using ^{99m}Tc and ^{67}Ga, in both phantoms and clinical studies.

Methods: Phantom studies were performed to evaluate planar and SPECT image contrast, spatial resolution, count rate performance and attenuation correction. Clinical bone images and gallium images were acquired with and without EWA and were evaluated for anatomical and lesion definition.

Results: For ^{99m}Tc, EWA was found to provide improved image contrast for both planar and SPECT images, with no deterioration in count rate performance and a small improvement in spatial resolution when compared to conventional on-peak and off-peak imaging. For ^{67}Ga, EWA was superior to conventional imaging using the lower two peaks, which in turn provided better contrast than using all three peaks.

Conclusion: The improvement in contrast in the phantom data was reflected in the clinical images. EWA images demonstrated greater anatomical definition in 60/65 ^{99m}Tc bone scans and in 20/22 ^{67}Ga scans.

Key Words: energy-weighted acquisition; attenuation correction; spatial resolution; bone imaging; gallium imaging

J Nucl Med Technol 1995; 23:49–55

In conventional nuclear medicine imaging systems a significant proportion of the emitted gamma rays that are used to form an image undergo Compton scattering within the patient. These scattered photons reduce image contrast. A number of methods have been proposed to reduce the contribution of the scattered radiation to the final image. These include: centering the pulse-height analyzer window 5% above the energy of the primary photon (known as off-peak imaging) (*1*); subtraction of a scaled "scatter image" obtained from a pulse-height window over the Compton energy distribution (*2*); splitting the photopeak window into two equal windows and determining the scatter contribution from the ratio of the counts in each window (*3*); and holospectral imaging in which the scattered counts in the photopeak are predicted from the total energy spectrum (*4*).

One of the few commercially available methods is known as energy-weighted acquisition (EWA) (*5,6*). This technique can be obtained from Siemens (Siemens Gammasonics, Inc., Des Plaines, IL) as an optional module for their Orbiter and Diacam gamma cameras and is known as the weighted acquisition module (WAM).

In evaluating EWA, Devito et al (*5*) demonstrated an improvement in image contrast in phantom studies. They concluded that EWA was a practical technique that addressed the problem of Compton scatter. Halama et al. (*7*) found that EWA resulted in an improvement in contrast by as much as 40% in both planar and SPECT imaging using ^{99m}Tc, ^{201}Tl and ^{67}Ga.

This paper provides a quantitative assessment of the overall performance of energy-weighted acquisition in phantom studies for ^{99m}Tc and ^{67}Ga, for both planar and tomographic images. In addition we have compared the qualitative image contrast from clinical images obtained using EWA, conventional on-peak imaging and off-peak imaging.

THEORY OF ENERGY-WEIGHTED ACQUISITION

Conventional gamma camera systems employ single channel pulse-height analyzers to accept photons within a fixed-energy window centered on the photopeak. All photons with energies in the accepted range make an equal contribution to the final image. Any photon whose energy falls outside this window is discarded. For example, a 20% window for ^{99m}Tc would accept all detected photons whose energy is in the range 126–154 keV. However a detected photon with a pulse-height equivalent to 140 keV is much more likely to be a true unscattered photon than is a detected photon with a pulse-height at 126 keV.

EWA is a technique in which every detected photon is given a weighting factor which is energy dependent. Thus, energies around the photopeak are assigned large positive values, whereas energies corresponding to scattered photons

For correspondence and reprints contact: Dr. R. C. Smart, Dept. of Nuclear Medicine, St. George Hospital, Kogarah, NSW 2217, Australia.

are given negative values. The Siemens WAM includes energy weighting functions, for ^{99m}Tc, ^{67}Ga and ^{201}Tl, that have been optimized to reduce the scatter contribution from these radionuclides over a range of organ depths found in a typical clinical environment. The weighting functions result in fractions of counts which are stored in two memory buffers until the count in any pixel exceeds one. At that time a single count is added to the corresponding pixel in the final image matrix and a count of 1.0 is subtracted from the buffer (*5*). The Siemens implementation allows a conventional or off-peak image to be acquired simultaneously with the energy-weighted image, enabling direct comparisons to be made.

MATERIALS AND METHODS

All images were acquired using a Diacam rectangular field-of-view gamma camera interfaced to an ICON computer (Siemens Gammasonics, Inc., Des Plaines, IL). The WAM module was calibrated daily according to the manufacturer's instructions.

The energy weighting functions provided by Siemens were derived for a single-scatter depth typical of abdominal imaging. It has been shown, however, that significant scatter reduction can be achieved using these weighting functions over a range of organ depths (*6*). These functions may not be appropriate for situations where there are less scattered photons present, such as bone imaging of the peripheral skeleton. In routine clinical practice, however, it is likely that EWA would be used for all images of a patient's study irrespective of the amount of overlying tissue. EWA has therefore been assessed in phantom studies in both scatter and nonscatter situations.

Phantom Studies

Planar Image Contrast. The phantom studies employed an acrylic contrast phantom, modified from the design of Murray et al. (*8*), in which solid rectangular blocks of varying heights and sizes allow for the assessment of both contrast and resolution (Fig. 1). The blocks varied in width from 10 mm to 20 mm and in true contrast from 45% to 100%. The phantom was filled with water containing 100 MBq of ^{99m}Tc and images were acquired using the LEAP collimator, with and without additional scattering material (50 mm anteriorly and 100 mm posteriorly). The images were collected using a 256 × 256 matrix employing a 3× zoom. A series of image pairs was collected simultaneously using either EWA and a 20% window centered on the 140 keV photopeak (which will be referred to as the on-peak image) or EWA and a 20% window centered on 148 keV (the off-peak image). The image acquisitions were repeated substituting 100 MBq of ^{67}Ga for the ^{99m}Tc, and using a medium energy collimator. In this case EWA was compared against conventional two-peak (93 keV, 180 keV) and three-peak (93 keV, 180 keV, 300 keV) imaging. In all cases, the images were acquired for 2M counts.

For the purpose of this study only the line of 15-mm width acrylic blocks in the images was analyzed. The image contrast of the blocks was determined from a three-pixel wide slice through the center of the blocks. The image contrast for the four blocks was calculated from the maxima and minima of the slice profile as:

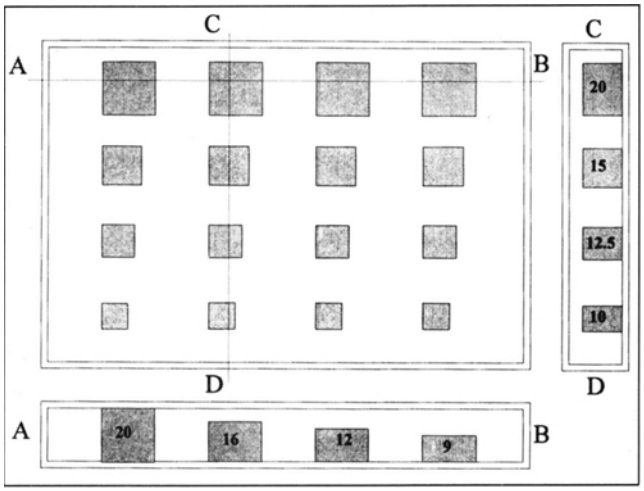

FIGURE 1. A schematic diagram of the phantom used to assess the image contrast. Each horizontal row consisted of square acrylic blocks of varying height. The blocks in each vertical row were of the same height but of varying cross-section. The numbers in the blocks represent their dimensions in millimeters.

$$\text{contrast} = \frac{\text{maximum} - \text{minimum}}{\text{maximum}} \times 100\% \qquad \text{Eq. 1}$$

Planar Spatial Resolution. The spatial resolution of the imaging system with the LEAP collimator was determined by measurement of the line spread function at increasing depths. A line source containing 90 MBq of ^{99m}Tc was placed at an angle of 45° in a 270-mm deep water tank. The surface of the collimator was 20 mm from the surface of the water. Images were obtained in a 256 × 256 matrix using EWA, on-peak and off-peak, collecting 2M counts in each case. Single-pixel wide profiles were obtained perpendicular to the axis of the line source for each pixel along the line, corresponding to depths of 0–270 mm. The resolution at a particular depth was determined by measuring the full width at half maximum (FWHM) of a Gaussian fit to the profile corresponding to that depth.

This study was repeated using ^{67}Ga with a medium energy collimator. In this second study, EWA was compared to two-peak and three-peak imaging.

Count Rate Performance. The quantitative accuracy of the EWA acquisition over a range of count rates was assessed by analyzing a dynamic study of a decaying source acquired using EWA and comparing this to the analysis of on- and off-peak studies collected under identical conditions using the LEAP collimator. The initial activity of the sources was chosen to approximate the range of count rates found in clinical images using ^{99m}Tc (1.5K counts/sec to 20K counts/sec). Images were acquired at a rate of one frame every four minutes using a 64 × 64 matrix.

Attenuation Correction. The attenuation coefficient for ^{99m}Tc in tissue-equivalent material was evaluated using a point source containing 20 MBq. This was supported in a water tank, initially at the surface of the water and then at 20-mm increments in depth. A five-minute image was obtained at each depth using EWA. The recorded counts were first corrected for radioactive decay and then plotted on a log scale against depth, to determine the linear attenuation coefficient.

SPECT Image Contrast. A SPECT phantom was filled with water containing 150 MBq of ^{99m}Tc. The phantom consisted of "cold" objects (rods and spheres) in a uniform background activity, "hot" objects in a cold background, and a linearity grid. Tomographic studies were performed using a 360° circular rotation, 128 frames each of 15 sec, and a matrix size of 128 × 128 pixels. Each planar projection image contained approximately 90K counts using a LEAP collimator. SPECT acquisitions were performed using EWA, on- and off-peak imaging. The data were reconstructed using a Butterworth filter of order 5, with a cutoff of 0.35 cycles/pixel and with attenuation correction using the previously determined attenuation coefficient. The data were reformatted as two-pixel thick transverse images. The image contrast through the cold rods of the phantom was found by measuring the minimum count and the average counts from the surrounding water from a three-pixel wide profile through the center of each observed cold rod, enabling the contrast to be calculated from Equation 1.

Patient Studies

Sixty-five ^{99m}Tc-MDP bone studies, comprising both whole-body and static images, were collected using either EWA with on-peak imaging (33 patients) or EWA with off-peak imaging (32 patients). In each case, the low-energy high-resolution collimator was used. The whole-body images were acquired for 15 min collecting between 2M and 3M counts per image, while the static images were collected for a total of 800K counts. Similarly, 22 ^{67}Ga studies including whole-body and static views were acquired using EWA and three-peak imaging (medium energy collimator, 500K count images). All images were displayed using the standard departmental protocol and were recorded on clear-base x-ray film. Two blinded observers independently viewed the paired images and graded the images as follows:

a. which image had better anatomical definition? EWA, on/off peak or neither
b. which image had better lesion definition? EWA, on/off peak or neither

RESULTS

Phantom Studies

Planar Image Contrast. In Figures 2A and 2B the ratio of the measured contrast to the true contrast for the 15-mm objects in the contrast phantom are plotted against their true contrast for each of the EWA, on-peak and off-peak images acquired using ^{99m}Tc. Using tissue-equivalent scatter material both anterior and posterior to the phantom, EWA demonstrated superior contrast at all object sizes and off-peak was superior to on-peak. When the phantom was imaged without additional scattering material, EWA was again superior in contrast but the difference was less marked, and for some objects, the EWA images gave a contrast ratio of greater than one. Figure 3 illustrates the images obtained using ^{99m}Tc in the contrast phantom without additional scatter using EWA (upper images), on-peak (lower left) and off-peak (lower right).

The contrast results for ^{67}Ga are presented in Figures 2C and 2D. In the presence of scattering material, EWA showed superior contrast at all object sizes when compared to two-peak imaging which was itself superior to three-peak imaging. In a scatter-free environment, two-peak imaging of ^{67}Ga gave the highest contrast over the middle range of object size while EWA contrast was greater at the extremes. Both two-peak and EWA were far superior to three-peak imaging for all object sizes. It must be noted that all the contrast values were much lower in the presence of the scattering medium than for the scatter-free situation.

Planar Spatial Resolution. The FWHM of the line source at varying depths in a tissue-equivalent material (water) is presented in Figure 4 for ^{99m}Tc. Although the accuracy of the calculated FWHM deteriorated with depth due to the lower counting statistics, it can be seen clearly that the spatial resolution using EWA was smaller than for off-peak at all depths investigated. The results using on-peak are not shown, but were very similar to those obtained using off-peak. The FWHM of the ^{99m}Tc line source using EWA was 6.3 mm at 0-mm depth in the water tank (20 mm from the collimator surface). The corresponding values for on-peak and off-peak were 6.7 mm and 6.6 mm respectively.

Count Rate Performance. The count rate of a decaying ^{99m}Tc source was monitored for approximately four half-lives, from 20K counts/sec to 1.5K counts/sec. There was no difference in the apparent rate of decay using either EWA, on-peak or off-peak imaging. In each case the measured half-life was 6.0 hr, with no evidence of any deviation from a single-exponential decay.

Attenuation Correction. Using conventional on-peak imaging, the attenuation coefficient of ^{99m}Tc in a tissue-equivalent scatter medium (water) was measured to be 0.12 cm^{-1}. In comparison, the attenuation coefficient using EWA was found to be 0.15 cm^{-1}, which is the true attenuation coefficient for 140 keV photons using narrow-beam geometry, i.e. without the scatter component, although a shoulder was noted on the curve indicating that there was still a scatter component to the EWA data (Fig. 5).

SPECT Image Contrast. The contrast in the center of the largest cold rod (22.4 mm diameter), which ideally should be 100%, was found to be 69% with on-peak imaging, 73% with off-peak imaging and 89% with EWA. This improvement in contrast was seen in the smaller rods, although the measured contrast was progressively less as the rod size decreased.

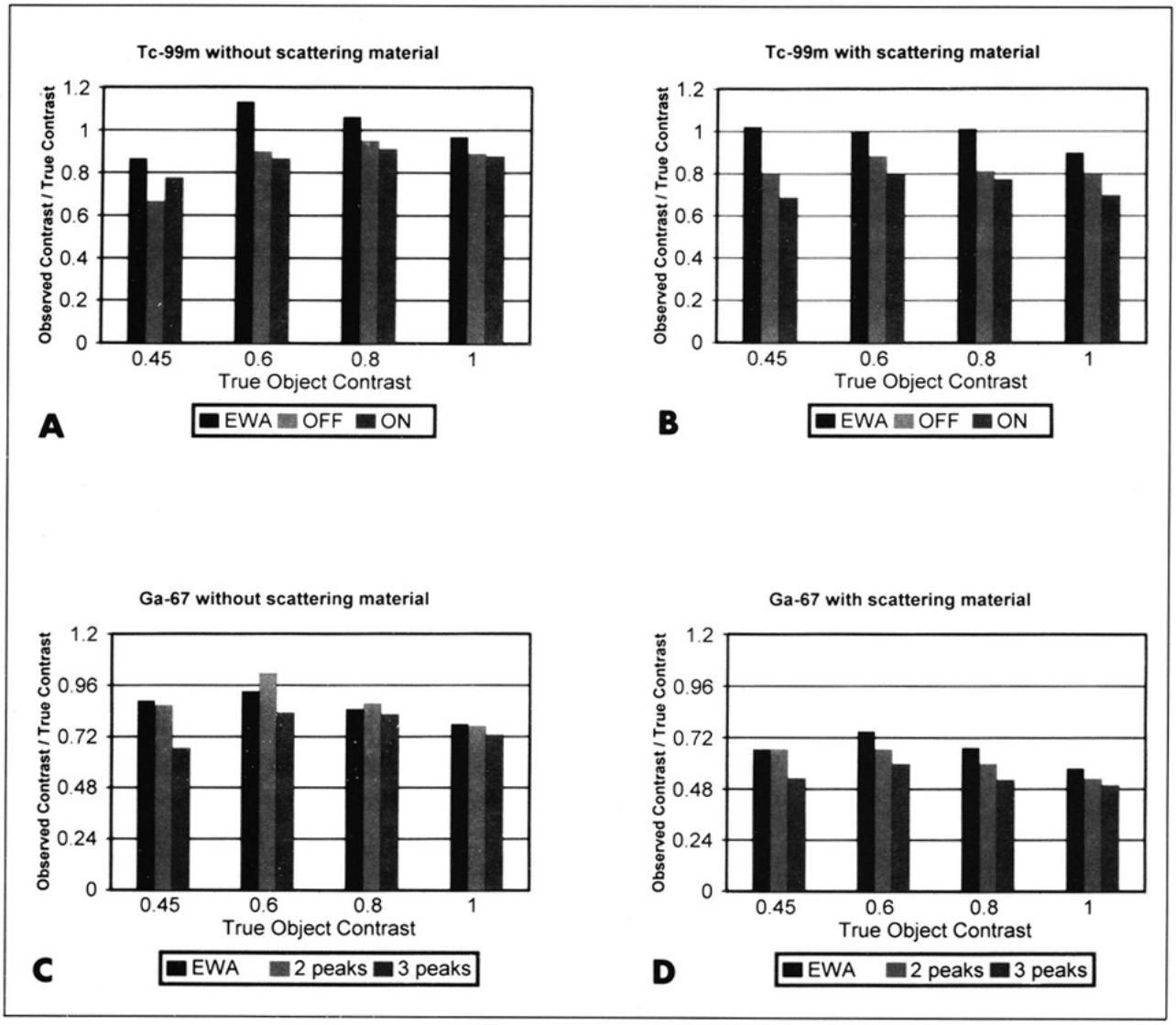

FIGURE 2. The ratio of the observed contrast to the true contrast for the 15-mm objects for four levels of true contrast. The top row of data (A and B) was obtained with ^{99m}Tc, the bottom row (C and D) with ^{67}Ga. The phantom was imaged with 50 mm of additional scatter material anteriorly and 100 mm posteriorly for graphs B and D.

Patient Studies

The two observers were in complete agreement on 92% (60 of 65) of the ^{99m}Tc-MDP bone scan cases. In these 60 cases, the observers indicated that EWA demonstrated greater anatomical definition due to improved contrast when compared to the on-peak images in 94% of the cases and to the off-peak images in 96% of the cases. Of the 22 ^{67}Ga images, agreement between observers was 91% (20 of 22) and, of these 20 cases, EWA was preferred in 86% of them. However there were no cases in either the ^{99m}Tc or ^{67}Ga images where the EWA images showed a lesion that was not apparent in the other acquired images. Examples of bone scans and gallium scans using EWA and conventional imaging are illustrated in Figures 6 through 10.

DISCUSSION

EWA has been shown to provide improved performance for all physical parameters measured: planar image contrast; planar spatial resolution at depth; SPECT image contrast; and attenuation correction. Furthermore the count rate using EWA remained quantitatively accurate over the full range of count rates typically experienced in a clinical setting.

EWA attempts to remove the influence of scattered photons by varying the weighting factors for the photons of different energies within the conventional photopeak window, and by giving negative weighting to photons with energies below the photopeak. Not only was image contrast improved using EWA but the measured attenuation coefficient for ^{99m}Tc was identical to that usually obtained under narrow-beam geometry situations, indicating that EWA had been effective in reducing the effects of scattered photons. The phantom results with ^{67}Ga also demonstrated a marked improvement in contrast using EWA. However, it should be noted that, when the phantom was imaged surrounded by tissue-equivalent scattering material,

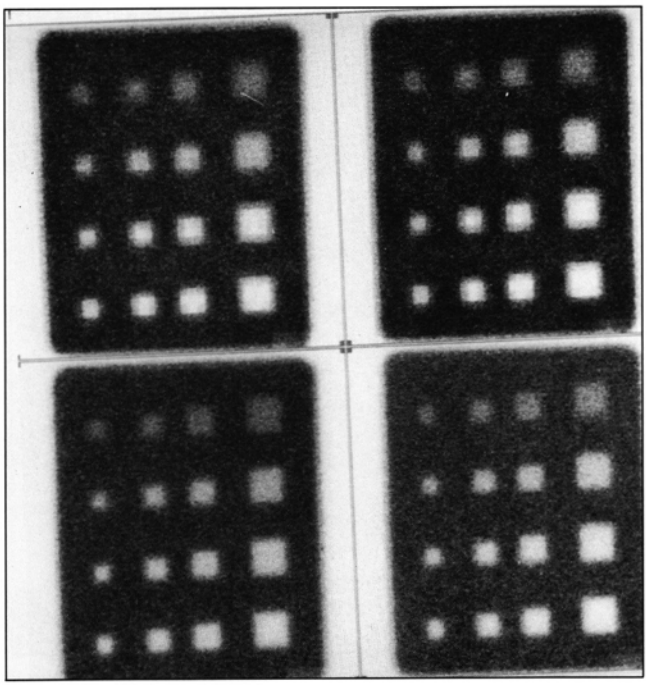

FIGURE 3. Images of the contrast phantom obtained with ^{99m}Tc, without additional scatter. The upper images were obtained using EWA, lower left with on-peak and lower right with off-peak imaging.

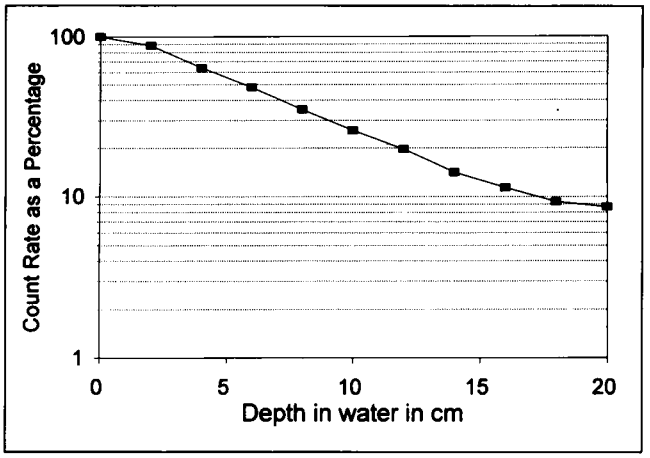

FIGURE 5. A plot of the count rate versus depth for a ^{99m}Tc point source imaged in a water tank. The linear attenuation coefficient calculated from mono-exponential portion of the data was 0.15 cm^{-1}.

the contrast was not restored to that observed in the scatter-free situation, indicating that there was a substantial residual scatter component even with EWA.

The improvement in contrast in the phantom data was reflected in the clinical images. The two observers indicated that the EWA images demonstrated improved anatomical definition in 92% of the ^{99m}Tc bone scans, and in 86% of the

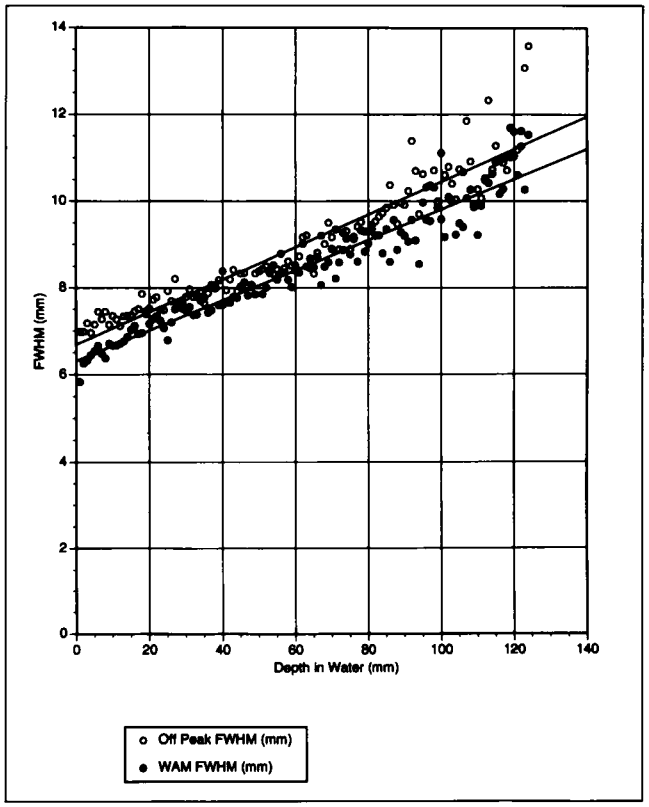

FIGURE 4. The measured FWHM of a ^{99m}Tc line source at each 1-mm increment in depth, imaged using off-peak and EWA. The results with on-peak were very similar to those obtained using off-peak.

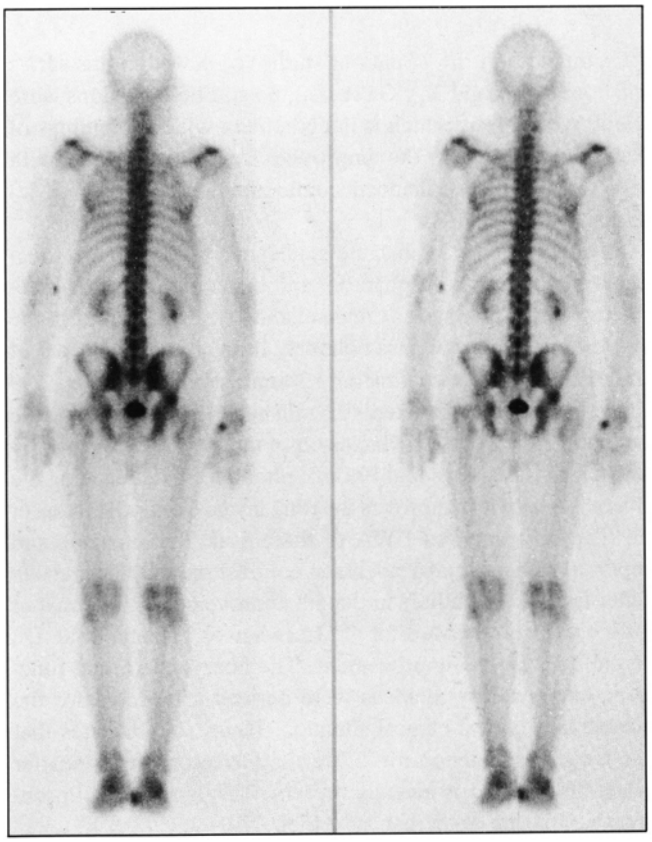

FIGURE 6. Posterior whole-body images using ^{99m}Tc-MDP acquired using on-peak (left) and EWA (right).

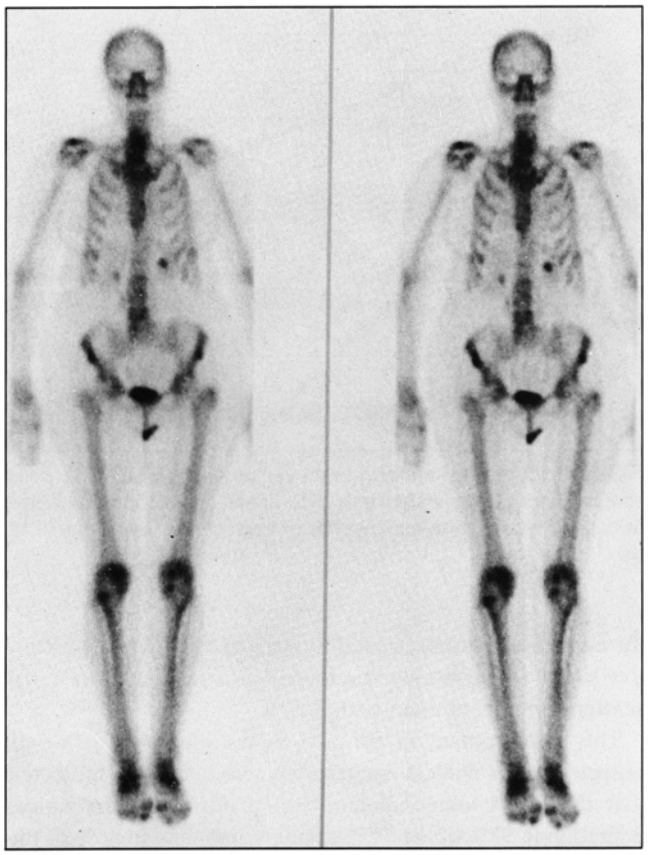

FIGURE 7. Anterior whole-body images using ^{99m}Tc-MDP acquired using off-peak (left) and EWA (right).

^{67}Ga images. Of the 77 patient studies reviewed in this series (65 bone scans and 22 ^{67}Ga scans), no additional lesions were found with EWA, which is in agreement with the findings of Rao (*9*). However, the improved contrast obtained with EWA resulted in enhanced confidence in the observed lesions.

The two-peak ^{67}Ga imaging studies were superior to three-peak imaging for both phantom and patient studies, in agreement with the findings of Currie et al. (*10*). Five percent of the 300 keV photons will pass obliquely through the lead septa of the medium energy collimator (1.14 mm septal thickness, 2.99 mm effective hole diameter, 40.6 mm hole length) degrading the resolution and contrast. Exclusion of the 300 keV photons, by only using the 93 keV and 180 keV photons, while reducing the overall sensitivity, improves the total image quality. Halama et al. (*7*) also compared EWA to three-peak ^{67}Ga imaging and reported similar improvements in contrast of 30%. Our results differ from these authors in that an improvement in contrast of 30% was also observed for ^{99m}Tc, whereas Halama et al. (*7*) found only an 8% improvement. The energy-weighting functions employed by Siemens were derived to account for the scatter in a typical clinical situation. Figure 2A indicates that the weighting function for ^{99m}Tc may overcorrect for scatter when little scatter is actually present. This may present problems in imaging of the hands or feet.

This study does not address the noise characteristics of images acquired using EWA. However this has been investigated by Jaszczak et al. (*11*), who demonstrated that the noise power spectra of EWA and on-peak images differed slightly. They concluded that their observed differences were unlikely to be of clinical significance.

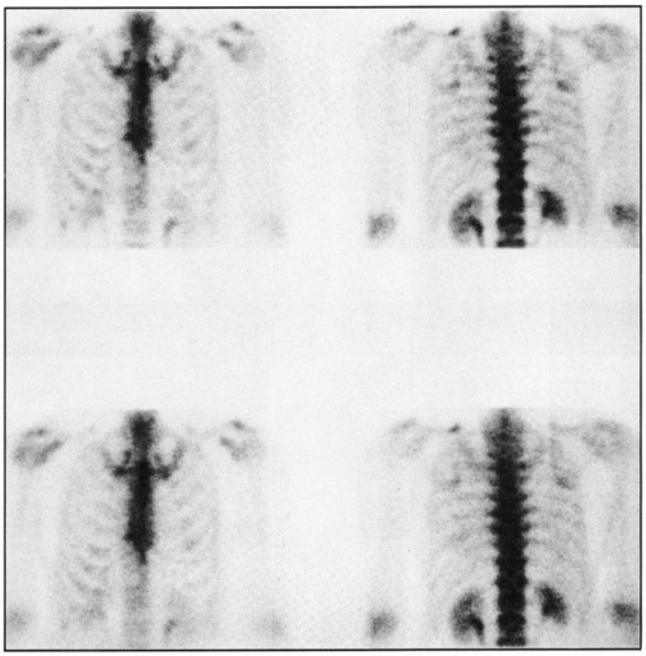

FIGURE 8. Planar static images of the anterior and posterior thorax using ^{99m}Tc-MDP acquired using EWA (top row) and off-peak (bottom row).

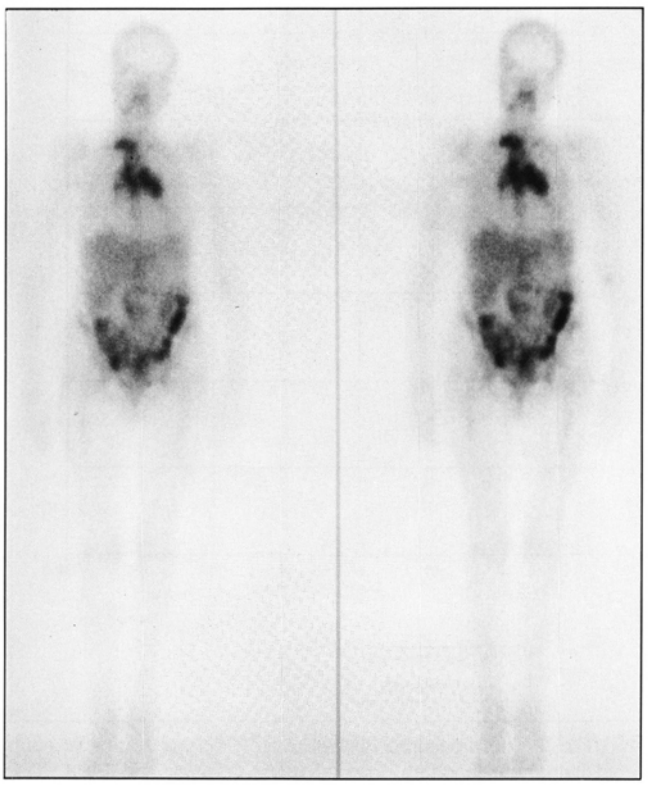

FIGURE 9. Anterior whole-body images using ^{67}Ga-citrate acquired using EWA (left) and three-peak imaging (right).

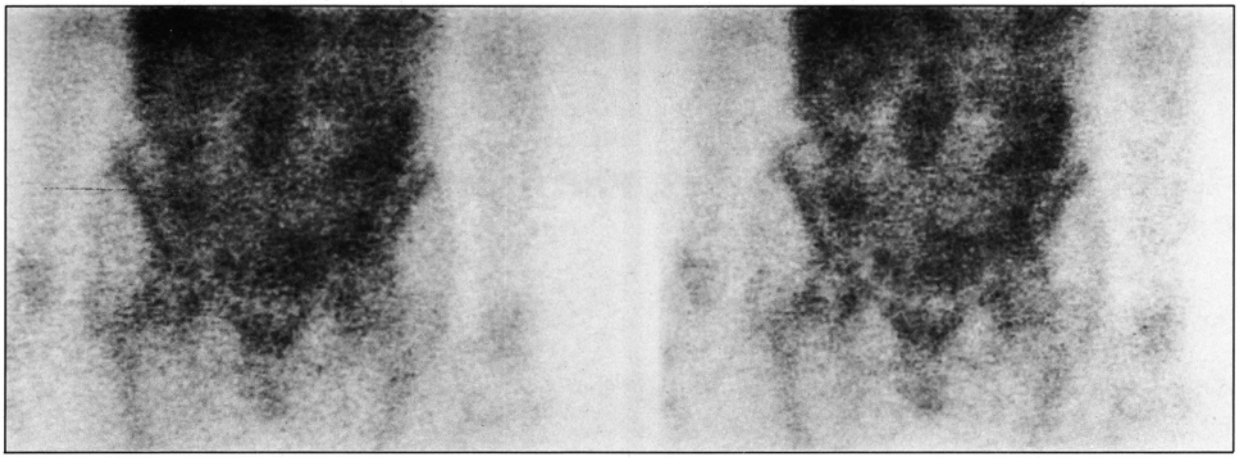

FIGURE 10. Anterior planar static images using ^{67}Ga-citrate acquired using three-peak imaging (left) and EWA (right).

CONCLUSION

EWA, obtained using the Siemens WAM, was found to give superior diagnostic images for both ^{99m}Tc and ^{67}Ga. If EWA is not available, off-peak imaging is preferable to on-peak imaging for ^{99m}Tc and two-peak imaging is preferable to three-peak imaging for ^{67}Ga.

REFERENCES

1. LaFontaine R, Graham LS, Stein MA. Effects of asymmetric photopeak windows on flood field uniformity and spatial resolution for scintillation cameras (Abstract). *J Nucl Med* 1984;25:P22.
2. Jaszczak RJ, Greer KL, Floyd Jr CE. Improved SPECT quantification using compensation for scattered photons. *J Nucl Med* 1984;25:893–900.
3. King MA, Hademenos GJ, Glick SJ. A dual-photopeak window method for scatter correction. *J Nucl Med* 1992;33:605–612.
4. Gagnon D, Todd-Pokropek A, Arsenault A, et al. Introduction to holospectral imaging in nuclear medicine for scatter subtraction. *IEEE Trans Med Imag* 1989;8:245–250.
5. DeVito RP, Hamill JJ, Treffert JD, et al. Energy-weighted acquisition of scintigraphic images using finite spatial filters. *J Nucl Med* 1989;30:2029–2035.
6. DeVito RP, Hamill JJ. Determination of weighting functions for energy-weighted acquisition. *J Nucl Med* 1991;32:343–349.
7. Halama JR, Henkin RE, Friend LE. Gamma camera radionuclide images: improved contrast with energy-weighted acquisition. *Radiology* 1988;169:533–538.
8. Murray KJ, Elliott AT, Wadsworth J. A new phantom for the assessment of nuclear medicine imaging equipment. *Phys Med Biol* 1979;24:188–192.
9. Rao MG. Bone imaging with energy-weighted acquisition. *J Nucl Med* 1993;34:997–999.
10. Currie GM, Meikle SR, McLaughlin AF, et al. Assessment of ^{67}Ga scanning using two and three energy windows. *Australian and New Zealand J Med* 1991;21:627.
11. Jaszczak RJ, Hoffman DC, DeVito RP. Variance propagation for SPECT with energy-weighted acquisition. *IEEE Trans Nucl Sci* 1991;38:739–747.

Please see end of second continuing education article, by Glowniak, for CE tests questions, answer sheet and answers to the March 1995 CE test.